JACS
JOURNAL OF THE AMERICAN CHEMICAL SOCIETY

ARTICLE

pubs.acs.org/JACS

β-$AgAl_{1-x}Ga_xO_2$ Solid-Solution Photocatalysts: Continuous Modulation of Electronic Structure toward High-Performance Visible-Light Photoactivity

Shuxin Ouyang[†] and Jinhua Ye[*,†,‡]

[†]Photocatalytic Materials Center (PCMC) and [‡]International Center for Materials Nanoarchitectonics, National Institute for Materials Science (NIMS), 1-2-1 Sengen, Tsukuba, Ibaraki 305-0047, Japan

Supporting Information

ABSTRACT: A series of β-$AgAl_{1-x}Ga_xO_2$ solid-solution materials were explored as novel visible-light-sensitive photocatalysts. These Ag-based solid solutions crystallize in a homogeneous crystal structure with orthorhombic symmetry but possess continuously modulated band gaps from 2.19 to 2.83 eV by decreasing the ratios of Ga/Al. Their photoactivities for iso-propanol degradation were found to be dependent on the variation of chemical compositions. Among them, the β-$AgAl_{0.6}Ga_{0.4}O_2$ sample showed the highest photocatalytic performance, which simultaneously exhibited 35 and 63 times higher activities than two terminus materials, β-$AgAlO_2$ and β-$AgGaO_2$, respectively. The apparent quantum efficiency of this sample for iso-propanol photodegradation achieved up to 37.3% at the wavelength of 425 ± 12 nm. The theoretical calculation based on density functional theory demonstrated that the levels of valence band maximum of β-$AgAl_{1-x}Ga_xO_2$ are similar, but the levels of conduction band minimum are gradually negatively shifted with the increase of the ratio of Ga/Al, thereby continuously narrowing the band gap. Nevertheless, the highest activity observed on β-$AgAl_{0.6}Ga_{0.4}O_2$ may be attributed to its optimized band structure, which adapts the balance between effective visible-light absorption and adequate redox potentials.

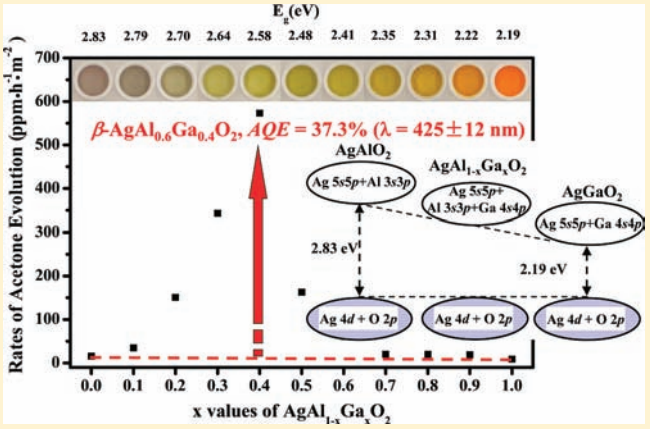

INTRODUCTION

Photocatalysis is an environmentally-friendly technology, which can supply an ambient-temperature process to completely decompose organic contaminants, split water to produce clean hydrogen energy, and convert CO_2 to hydrocarbon fuel using solar light.[1−6] Thus it will potentially be embraced into the future sustainable-development strategy. From the view of effectively utilizing solar energy, developing highly efficient visible-light-sensitive photocatalysts is highly anticipated and thus has attracted extensive attention. During recent decades, various semiconductor materials, including modified-TiO_2,[7−11] multimetal oxides,[12−14] sulfides,[15,16] oxynitrides,[17−19] and heterojunctions[20−22] have been successfully fabricated by diverse strategies of band-structure engineering, and their novel and unique photocatalytic properties have been extensively explored.

To sensitize the photocatalysts into the visible region, their band gaps could be narrowed via lowering the level of the conduction band, lifting the level of the valence band, or both, which at the same time generally suppresses the redox potentials. Accordingly, it inevitably causes an implicit contradiction between the wide visible-light absorption and the adequate redox capability. In this sense, modulation of electronic structure to achieve an optimized balance between light absorption and redox potential is one feasible approach to minimize this contradiction. In early studies, the methods of doping and element substitution were widely explored, such as $InMO_4$ (M = V, Nb, and Ta),[23] $MCo_{1/3}Nb_{2/3}O_3$ (M = Ca, Sr, and Ba),[24] and $In_{0.8}M_{0.2}TaO_4$ (M = 3d transition metals).[25] However, it was difficult to attain a precise adjustment to their electronic structures. Thus, the fabrication of solid-solution photocatalysts with continuous band gaps emerged as being a requirement. Until now, this strategy has succeeded in many examples in the field of H_2 or/and O_2 evolution from water splitting,[15,18,26−28] but for the elimination of organic contaminants, limited progress has been achieved.[28,29]

Recently, Ag-based photocatalysts[28−36] have attracted wide research interest because the hybridization of Ag 4d and O 2p states in the valence band can easily extend light absorption into the visible region while maintaining a strong oxidization potential. Accordingly, we have been devoting efforts to explore new Ag-based photocatalysts.[28−30,33−36] As a typical example, we recently developed a novel visible-light-sensitive photocatalyst,

Received: November 29, 2010
Published: March 10, 2011

dx.doi.org/10.1021/ja110691t | J. Am. Chem. Soc. 2011, 133, 7757–7763

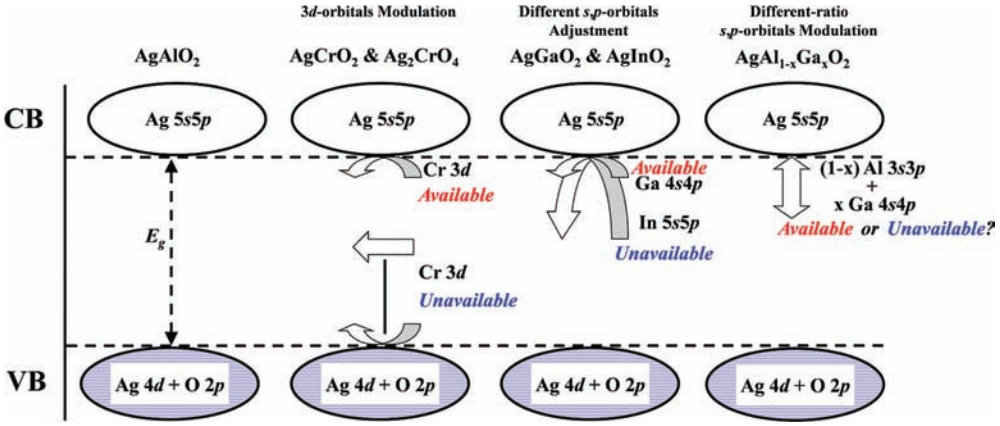

Figure 1. Strategies to modulate band structures of ABO_2-type Ag-based oxide photocatalysts for the previous and present studies.

Ag_3PO_4, which exhibits extremely high photooxidative capability for O_2 evolution from water as well as organic dye decomposition under visible light irradiation. More specifically, this novel photocatalyst can achieve quantum efficiency up to 80% in the visible region of 400−480 nm.[36] Furthermore, we systematically studied the effects of crystal structure and electronic structure of $AgMO_2$ (M = Al, Ga, and In) on photocatalytic activity. It was found that the $AgMO_2$ oxides were a series of photocatalysts with the capability of photooxidizing organic compounds.[34] This work aims to carry out a strategy of fabricating solid-solution photocatalysts to further enhance the photocatalytic efficiency of the $AgMO_2$ oxide system. However, how to improve the band structure, through modulating the conduction band, adjusting the valence band, or both, remains a question. A review of our former studies helps us to inspire the feasible approach. As illustrated in Figure 1, in the $AgMO_2$ oxide system, the β-$AgAlO_2$ was first developed as a visible-light-sensitive photocatalyst to degrade organic dye in aqueous solution and decompose gaseous organic pollutant, but its activity was not high because of the relatively wide band gap.[30] To increase the visible-light absorption, Cr with different chemical valences has been used to substitute the Al of $AgAlO_2$. A comparative study of the electronic structures of $AgCrO_2$ and $AgCr_{1/2}O_2$ (Ag_2CrO_4) demonstrated that introducing occupied 3d states into the valence band greatly reduced the oxidization potential and thus made the material inactive.[33] Therefore, lowering the level of the conduction band is the only feasible way to enhance visible-light photocatalytic activity. We further substituted Al by Ga or In to detect the limitation of conduction-band modulation. Among four materials of two different phases, the α-$AgInO_2$ showed the lowest activity for the photooxidization of gaseous organic contaminant, indicating that participation of In 5s5p states into the conduction band significantly weakened the reduction potential and subsequently made the catalyst inefficient.[34] More effective improvement is expected to fabricate α-$AgAl_{1-x}Ga_xO_2$ or β-$AgAl_{1-x}Ga_xO_2$ solid solutions to continuously modulate the conduction band via adjusting the ratios of Al 3s3p and Ga 4s4p states. In this work, the β-$AgAl_{1-x}Ga_xO_2$ solid-solution photocatalysts were prepared by a two-step route. The iso-propanol (IPA) photodegradation over these photocatalysts under visible-light irradiation was investigated to test the validity of the strategy of making solid solution. The further theoretical calculation helped to clarify the variation of electronic structure and subsequently understand the relation between photocatalytic activity and electronic structure.

EXPERIMENTAL SECTION

Material Preparation. β-$AgAl_{1-x}Ga_xO_2$ was synthesized via a cation-exchange method of treating $NaAl_{1-x}Ga_xO_2$ with molten $AgNO_3$. The precursor, $NaAl_{1-x}Ga_xO_2$, was prepared by a sol−gel approach. Briefly, stoichiometric CH_3COONa (98.5%), $Al(NO_3)_3\cdot 9H_2O$ (98%), and $Ga(NO_3)_3\cdot nH_2O$ (n = 7−9) (99.9%) were dissolved in ethylene glycol and heated to 60−70 °C for 8−12 h to form white or brown gel. The obtained gel was further treated at 200 °C for 10 h and further calcined at 900 °C for 12 h into crystallized $NaAl_{1-x}Ga_xO_2$ solid solution. After that, the cation-exchange reaction was carried out by heating the mixture of $NaAl_{1-x}Ga_xO_2$, $AgNO_3$ (99.8%), and KNO_3 (99.0%), with a molar ratio of 1.00: 1.03: 1.00, at 210 °C for 20 h, among which KNO_3 was used as a fluxing medium to prevent the side reduction of Ag^+ to Ag^0.[37] The product was washed repeatedly with distilled water to remove $NaNO_3$, KNO_3, and excess $AgNO_3$. Finally, the β-$AgAl_{1-x}Ga_xO_2$ sample was dried in air at room temperature. A flow chat of synthesis for the β-$AgAl_{1-x}Ga_xO_2$ samples is included in Supporting Information, SI-1.

Sample Characterization. Structural features of the specimens were determined using powder X-ray diffraction (RINT-2000; Rigaku Corp., Japan) with Cu $K\alpha_1$ radiation. The diffuse reflectance spectra of the samples were recorded on a UV−visible spectrophotometer (UV-2500PC; Shimadzu Corp., Japan) with barium sulfate as the reference. Then the absorption spectra were obtained from the reflectance spectra by means of Kubelka−Munk transformations. The Brunauer−Emmett−Teller (BET) surface areas were measured via nitrogen physisorption (Gemini2360; Micromeretics Corp., U.S.A.).

Activity Evaluation. A 300-W Xe arc lamp (7 A imported current, focused through a 45 ×45 mm shutter window) was employed for the light source of photocatalytic reaction. The light beam was passed a set of glass filters (HA30 + U390 + L42, 400 nm < λ < 530 nm) and a water filter (removing the infrared ray irradiation) before reaching the reactor (the spectral profiles of Xe arc lamp with and without filters are shown in Supporting Information, SI-2). The reactor volume was 500 mL; it was equipped with a Pyrex-glass lid as a window. Under such conditions, the incident light intensity was 0.46 mW/cm^2. The light intensities in the photocatalytic reaction were measured using a spectroradiometer (USR-40; Ushio Inc., Japan). The light intensity data were collected from 200 to 800 nm. The 350 mg of sample was spread uniformly on an 8.5 cm^2-plate which was placed in the bottom of the reactor. Then the reactor was pretreated by artificial air [$V(N_2)$: $V(O_2)$ = 4:1] for 5 min to remove adsorbed gaseous impurities. The iso-propanol (IPA) was injected into the reactor to produce a concentration of 1200−1500 ppm. Before irradiation, the reactor was kept in the dark until ensuring an adsorption−desorption equilibrium of gaseous reactants on the sample. The concentrations of IPA and acetone were detected on a gas chromatograph

dx.doi.org/10.1021/ja110691t |J. Am. Chem. Soc. 2011, 133, 7757–7763

(GC-14B; Shimadzu Corp., Japan) with an FID detector (Details: Porapak Q and PEG1000 column; temperatures—injection port, 120 °C; column, 60 °C; detection, 200 °C; maximum error about 7%). The measurements of apparent quantum efficiency were performed under similar conditions except for the wavelength regions of the incident light. Various glass filters consisting of cutoff and band-pass filters were used to control the wavelength regions of irradiation light. For every wavelength region, the irradiation lasted for 60 min. The IPA photooxidization undergoes two kinds of typical reaction processes as below:[38,39]

(1) one-photon reaction

$$CH_3CHOHCH_3 + e^- + O_2 + H^+ \rightarrow CH_3COCH_3 + HO\bullet + H_2O$$

$$\text{or } CH_3CHOHCH_3 + h^+ \rightarrow CH_3COCH_3 + 2H^+ + e^-$$

(2) multiphoton reaction

$$CH_3CHOHCH_3 + 5H_2O + 18h^+ \rightarrow 3CO_2 + 18H^+$$

Thus, the apparent quantum efficiency was calculated as the following equation,

$$AQE = [N(CO_2) \times 6 + N(\text{acetone})]/N(\text{photons}) \times 100\%$$

in which $N(CO_2)$, N(acetone), and N(photons) signify the molecular number of generated CO_2 in unit time, the molecular number of generated acetone in unit time, and the number of incident photons in unit time, respectively. The long-term experiment and the contrast experiments with a commercial $TiO_{2-x}N_x$ (TPS201; Sumitomo Corp., Japan) as reference were performed under the irradiation of blue-LED lamps.

Theoretical Calculations. Electronic structures of the five models, β-$AgAlO_2$, β-$AgAl_{0.75}Ga_{0.25}O_2$, β-$AgAl_{0.5}Ga_{0.5}O_2$, β-$AgAl_{0.25}Ga_{0.75}O_2$, and β-$AgGaO_2$, were investigated via the plane-wave-pseudopotential approach based on the density functional theory (DFT). For β-$AgAl_{0.75}Ga_{0.25}O_2$, β-$AgAl_{0.5}Ga_{0.5}O_2$, and β-$AgAl_{0.25}Ga_{0.75}O_2$, various geometry optimization models were performed to determine the most stable structures, respectively (as shown in Supporting Information, SI-3). Then their electronic structures were calculated using a standard Cambridge serial total energy package (CASTEP) code.[40] The electron—core interaction was represented via ultrasoft pseudopotentials with a plane-wave basis cutoff energy of 340 eV. The electronic exchange-correlation energy was treated within the framework of the local density approximation (LDA). The self-consistent field (SCF) tolerance was all 1×10^{-6} eV/atom. The FFT grids of basis in all the models were $30 \times 40 \times 30$. The k-point sets of $5 \times 4 \times 5$ were used for all the models.

RESULTS AND DISCUSSION

Synthesis and Crystal Structural Characteristic. Cation-exchange reaction by using Na-based precursors was proven to be an effective method in preparing Ag-based material.[30,31,33−36] In this work, the $NaAl_{1-x}Ga_xO_2$ solid-solution precursors were prepared by a sol—gel approach instead of solid-state reaction, since the solid-state process made it difficult to generate a single-phase precursor. Then, these precursors were treated with molten $AgNO_3$ and KNO_3 to produce the β-$AgAl_{1-x}Ga_xO_2$ solid solutions. The XRD patterns of the β-$AgAl_{1-x}Ga_xO_2$ solid solutions in Figure 2 show that all of the samples have a homogeneous crystal structure with orthorhombic symmetry (see calculated lattice parameters in Table 1), which belongs to a typical cristobalite-related structure[41] (Figure 3). With varying x from 0 to 1.0, all diffraction peaks gradually shift to smaller

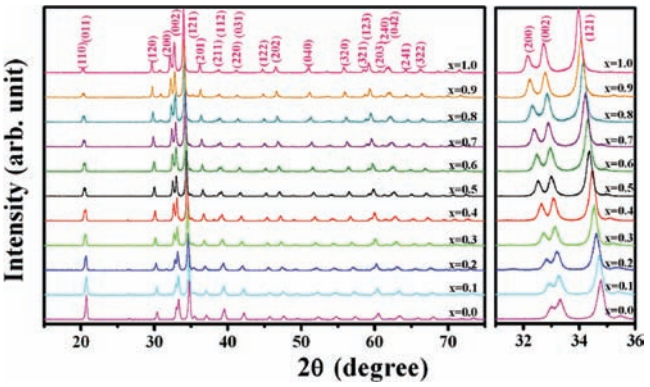

Figure 2. XRD patterns of β-$AgAl_{1-x}Ga_xO_2$ solid solutions.

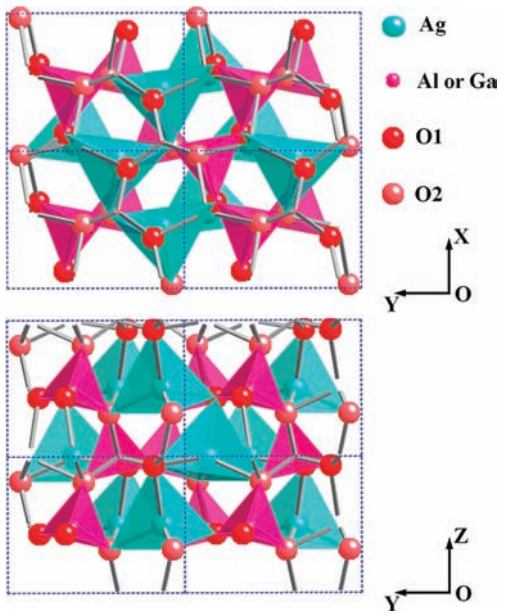

Figure 3. Schematic crystal structure of β-$AgAl_{1-x}Ga_xO_2$ solid solutions.

angles. The enlarged image of Figure 2 illustrates the change of the three strongest peaks. When x value increases, the peaks that represent the crystal plane (2 0 0) and (0 0 2) clearly separate each other, which can be ascribed to the faster variation of a-lattice axis than that of the c-lattice axis (the slope of $a = a(x)$ is 0.14, whereas that of $c = c(x)$ is 0.10, see more details in the Supporting Information, SI-4). The regular evolution of the XRD patterns reveals that the as-prepared samples are a group of continuous solid solutions. The morphologies of the β-$AgAl_{1-x}Ga_xO_2$ solid solutions were investigated by SEM. It can be found that the as-prepared samples are all irregular particles with sizes around 200 nm to 10 μm (as shown in Supporting Information, SI-5).

Photophysical and Photocatalytic Properties. Figure 4 displays UV—visible absorption spectra of the β-$AgAl_{1-x}Ga_xO_2$ samples. All of these oxides possess absorption edges that extend into the visible region. With gradually substituting Al with Ga, the absorption edges show continuous red-shifts. Their band gaps are calculated by equation of $\alpha h\nu = A(h\nu - E_g)^{n/2}$, in which α, ν, A, and E_g, respectively, signify the absorption coefficient, light frequency, proportionality constant, and band gap, and n equals

dx.doi.org/10.1021/ja110691t |J. Am. Chem. Soc. 2011, 133, 7757–7763

Table 1. Crystal Structures and Photophysical and Photocatalytic Properties of β-$AgAl_{1-x}Ga_xO_2$

material	crystal systems	lattice parameters (Å)			band gaps (eV)	surface areas (m^2/g)	acetone evolution [ppm/(h-m^2)]
$AgAlO_2$	orthorhombic	a = 5.426(2)	b = 6.996(3)	c = 5.378(2)	2.83	2.2	16
$AgAl_{0.9}Ga_{0.1}O_2$	orthorhombic	a = 5.439(2)	b = 7.001(3)	c = 5.388(2)	2.79	2.2	35
$AgAl_{0.8}Ga_{0.2}O_2$	orthorhombic	a = 5.456(2)	b = 7.021(3)	c = 5.395(2)	2.70	2.1	151
$AgAl_{0.7}Ga_{0.3}O_2$	orthorhombic	a = 5.473(2)	b = 7.042(3)	c = 5.403(3)	2.64	2.6	343
$AgAl_{0.6}Ga_{0.4}O_2$	orthorhombic	a = 5.489(2)	b = 7.052(2)	c = 5.417(2)	2.58	2.7	573
$AgAl_{0.5}Ga_{0.5}O_2$	orthorhombic	a = 5.503(2)	b = 7.073(3)	c = 5.425(2)	2.48	3.2	163
$AgAl_{0.4}Ga_{0.6}O_2$	orthorhombic	a = 5.512(1)	b = 7.089(2)	c = 5.436(2)	2.41	2.2	61
$AgAl_{0.3}Ga_{0.7}O_2$	orthorhombic	a = 5.527(1)	b = 7.107(2)	c = 5.448(1)	2.35	2.6	20
$AgAl_{0.2}Ga_{0.8}O_2$	orthorhombic	a = 5.541(2)	b = 7.123(3)	c = 5.456(2)	2.31	2.5	20
$AgAl_{0.1}Ga_{0.9}O_2$	orthorhombic	a = 5.553(2)	b = 7.142(3)	c = 5.467(2)	2.22	2.4	19
$AgGaO_2$	orthorhombic	a = 5.568(1)	b = 7.162(2)	c = 5.477(2)	2.19	3.0	9

1 or 4, depending on whether the transition is direct or indirect, respectively.[42] Here n = 4 because the after-mentioned theoretical calculations reveal that these materials are all indirect-gap semiconductors (see details in Supporting Information, SI-6). The band gaps of the β-$AgAl_{1-x}Ga_xO_2$ samples are listed in Table 1. The linear tendency of the band gap variation also indicates that the β-$AgAl_{1-x}Ga_xO_2$ oxides form the continuous solid solutions.

The photocatalytic activities of as-prepared samples were evaluated by the degradation of gaseous IPA into acetone under visible-light irradiation. Under light irradiation, the photogenerated electrons of photocatalyst can combine with a molecule of O_2 to produce the $\bullet O_2^-$ radical, and then the $\bullet O_2^-$ oxidizes IPA to become acetone; or the photoexcited holes directly oxidize IPA into acetone.[38,39] Therefore, the photooxidization of IPA to acetone is a one-photon process. After that, the acetone could be further oxidized into CO_2 through a multielectron oxidization process.[38] The clear reaction mechanism and typical intermediate product enable us to evaluate relatively precise quantum efficiency and judge if photogenerated electrons and holes really participate in the photoreaction process or not. Therefore, the photocatalytic degradation of IPA was selected as a model reaction in this work. Figure 5 presents the evolution rates of acetone, band gaps, and colors of the β-$AgAl_{1-x}Ga_xO_2$ samples. The evolution rates of acetone from the IPA degradation are closely dependent on the chemical compositions of β-$AgAl_{1-x}Ga_xO_2$ solid solutions. The β-$AgAl_{0.6}Ga_{0.4}O_2$ with a band gap of 2.58 eV shows the highest activity for IPA photodegradation. The evolution rate of acetone over this material achieves 35 and 63 times of enhancement in comparison with two terminus materials, β-$AgAlO_2$ and β-$AgGaO_2$, respectively. Considering that light absorption is also a key factor for photoactivity, we normalized the photoactivity by the amount of absorbed photons. Similarly, the β-$AgAl_{0.6}Ga_{0.4}O_2$ still showed the highest performance among these solid solutions (see more details in Supporting Information, SI-7). For this sample, we measured the apparent quantum efficiency (AQE) of IPA converting into acetone and CO_2 (the measuring method is the similar to our previous report).[34] Figure 6 shows the wavelength dependence of AQE, which was often used to distinguish if the present chemical process is really a photocatalytic reaction or not. The light absorption of β-$AgAl_{0.6}Ga_{0.4}O_2$ extends to the visible region until about 480 nm. The additional absorption of λ > 480 nm is caused by metallic Ag impurity. It can be observed that the AQE decreases with increasing wavelength of incident light, which is consistent with the optical absorption of the present material. It not only indicates that the photophysical property of the

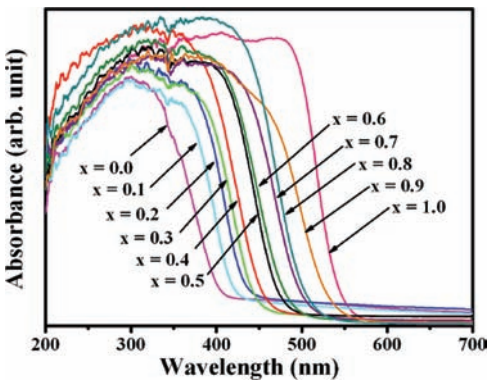

Figure 4. UV−visible absorption spectra of β-$AgAl_{1-x}Ga_xO_2$ solid solutions.

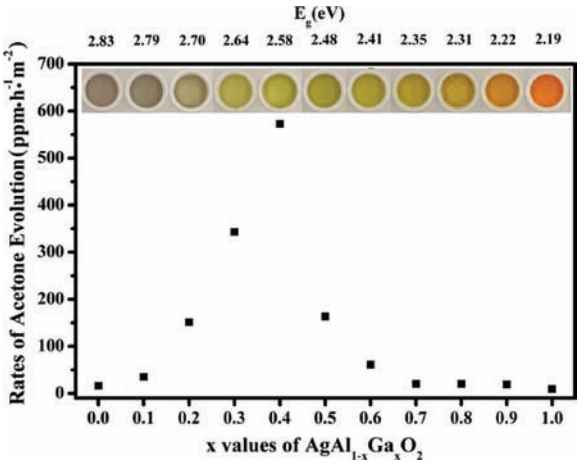

Figure 5. Evolution rates of acetone, band gaps, and colors of the β-$AgAl_{1-x}Ga_xO_2$ samples.

β-$AgAl_{0.6}Ga_{0.4}O_2$ oxide governs the chemical process of converting IPA into acetone and CO_2, but also suggests that the present reaction is a photocatalytic reaction. The AQE at the wavelength of 425 ± 12 nm of β-$AgAl_{0.6}Ga_{0.4}O_2$ achieves 37.3%, which is obviously higher than that of other reported Ag-based oxide photocatalysts.[28−34]

For comparison, we measured the photoactivities of β-$AgAl_{0.6}Ga_{0.4}O_2$ and a commercial $TiO_{2-x}N_x$ (the optical properties of

dx.doi.org/10.1021/ja110691t |J. Am. Chem. Soc. 2011, 133, 7757–7763

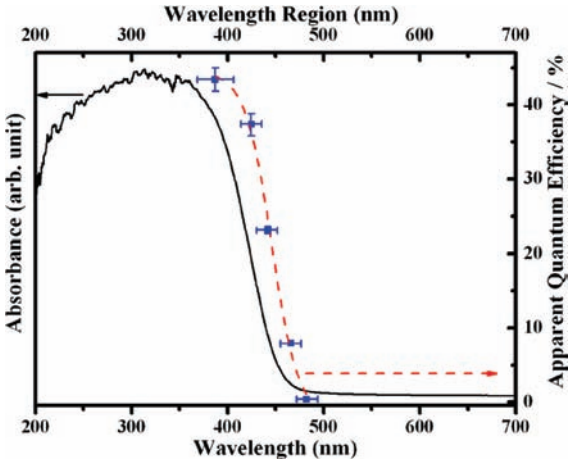

Figure 6. Apparent quantum efficiencies of IPA photodegradation over the β-$AgAl_{0.6}Ga_{0.4}O_2$ sample at various light wavelength ranges consistent with the UV−visible absorption spectrum. Horizontal error bar presents wavelength range; vertical error bar presents AQE error induced by light-intensity measurement.

these two samples are compared and shown in Supporting Information, SI-8) under the irradiation of blue-LED lamps, which could steadily supply the visible-light irradiation with a 10 $\mu W/cm^2$ intensity (similar to that of indoor illuminations). As shown in Figure 7, the rate of acetone evolution over β-$AgAl_{0.6}Ga_{0.4}O_2$ reaches 87% of $TiO_{2-x}N_x$, whereas the efficiency to produce CO_2 of the former one exceeds that of the latter one. The metallic Ag precipitated on the catalyst surface plays an important role in improving photocatalytic activity.[28] As the present synthetic process inevitably caused metallic Ag on sample surface, the higher activity for CO_2 evolution over β-$AgAl_{0.6}Ga_{0.4}O_2$ may be attributed to that the cocatalyst promotes the multielectron reaction process which benefits the completed photooxidization of IPA[43] ($C_3H_8O + 5H_2O + 18\ h^+ \rightarrow 3CO_2 + 18H^+$). As the surface area of a catalyst greatly affects its catalytic efficiency,[44] to keep the same surface area, a $TiO_{2-x}N_x$ sample (BET surface area, 64.8 m^2/g) with 15-mg mass was also evaluated for activity under the same conditions. In this case, the activity of β-$AgAl_{0.6}Ga_{0.4}O_2$ was obviously higher than that of $TiO_{2-x}N_x$. Therefore, the synthetic technique for increasing surface area of multimetal oxide is still in urgent need. A long-term IPA photodecomposition over β-$AgAl_{0.6}Ga_{0.4}O_2$ was also evaluated under the irradiation of blue-LED lamps. This material could continuously photooxidize IPA into acetone and then CO_2 (as shown in Supporting Information, SI-9).

The stability of this material was tested using powder XRD and UV−visible absorption spectrum (the results are shown in Supporting Information, SI-10). These measurements revealed that the crystal structures and band gaps of the as-prepared and postreaction samples did not change obviously. However, a slight uplift of the background in the UV−visible absorption spectrum was observed, which was probably attributed to a little amount of metallic Ag or deficiency appearing on the surface of photocatalyst after irradiation. Thus, the turnover number in terms of Ag ions in the surface is a necessary index to prove that the present reaction is a catalytic process. The turnover number of the reaction over β-$AgAl_{0.6}Ga_{0.4}O_2$ under the visible-light irradiation of Xe lamp ($400\ nm < \lambda < 530\ nm$) reached 4.2 in 2 h, which clearly indicates the present IPA photodegradation is photocatalytic reaction (for calculation details, see Supporting Information, SI-11).

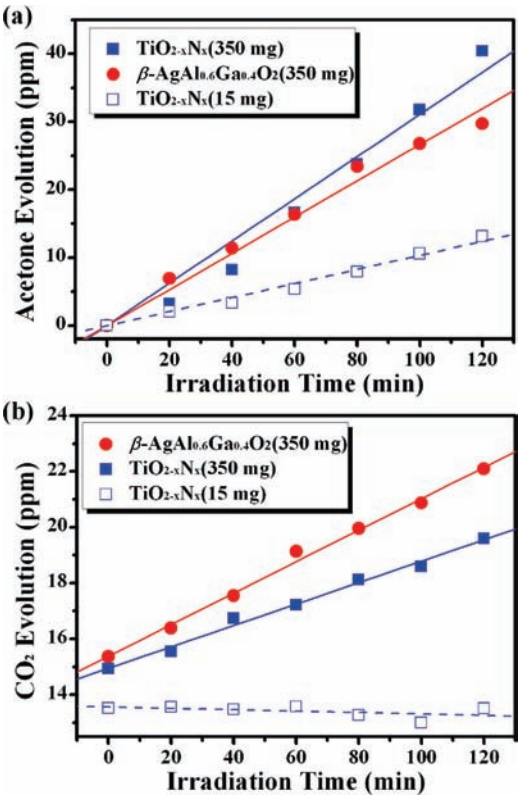

Figure 7. Acetone (a) and CO_2 (b) evolution over β-$AgAl_{0.6}Ga_{0.4}O_2$ and commercial $TiO_{2-x}N_x$ under irradiation of blue-LED lamps (light intensity, 10 $\mu W/cm^2$).

Electronic Structure. The electronic structure of a semiconductor photocatalyst plays an important role in the level of the conduction band and the valence band, which subsequently influences the photocatalytic performance. The theoretical calculation herein helps us understand the variation of photocatalytic activity in the β-$AgAl_{1-x}Ga_xO_2$ solid solutions. Figure 8 exhibits the electronic structures of β-$AgAlO_2$, β-$AgAl_{0.75}Ga_{0.25}O_2$, β-$AgAl_{0.5}Ga_{0.5}O_2$, β-$AgAl_{0.25}Ga_{0.75}O_2$, and β-$AgGaO_2$. The valence bands of β-$AgAl_{1-x}Ga_xO_2$ are all composed of Ag 4d and O 2p states, while the conduction bands are mainly constructed from Ag 5s5p, Al 3s3p, and Ga 4s4p states. Thus, the levels of valence band maximum (VBM) are similar, but the levels of conduction band minimum (CBM) are controlled by the ratio of Ga/Al. Since Ga 4s4p levels are lower than Al 3s3p levels (namely, the Ga 4s4p levels are positive than Al 3s3p levels relative to vacuum level), the substitution of Al by Ga induces a negative shift of CBM and subsequently narrows the band gap. The calculation is well consistent with the variation of the experimental band gaps.

It is acknowledged that the photocatalytic decomposition of the gaseous organic compounds in the presence of oxygen mainly involves: (1) by absorbing the incident photons, excitation of the electrons from VB to CB coincides the generation of the holes in VB; (2) the electrons contribute to reducing O_2 to form $\bullet O_2^-$ species; and (3) the organic molecules are oxidized by the holes or the surface •OH radicals.[1,13,38,39] On the basis of the aforementioned electronic-structure feature, the β-$AgAl_{1-x}Ga_xO_2$ oxides are typical electron-conductive semiconductors, since the Ag 4d states participate in the construction of VBM which induces relatively localized photoholes. Furthermore, the

dx.doi.org/10.1021/ja110691t |J. Am. Chem. Soc. 2011, 133, 7757–7763

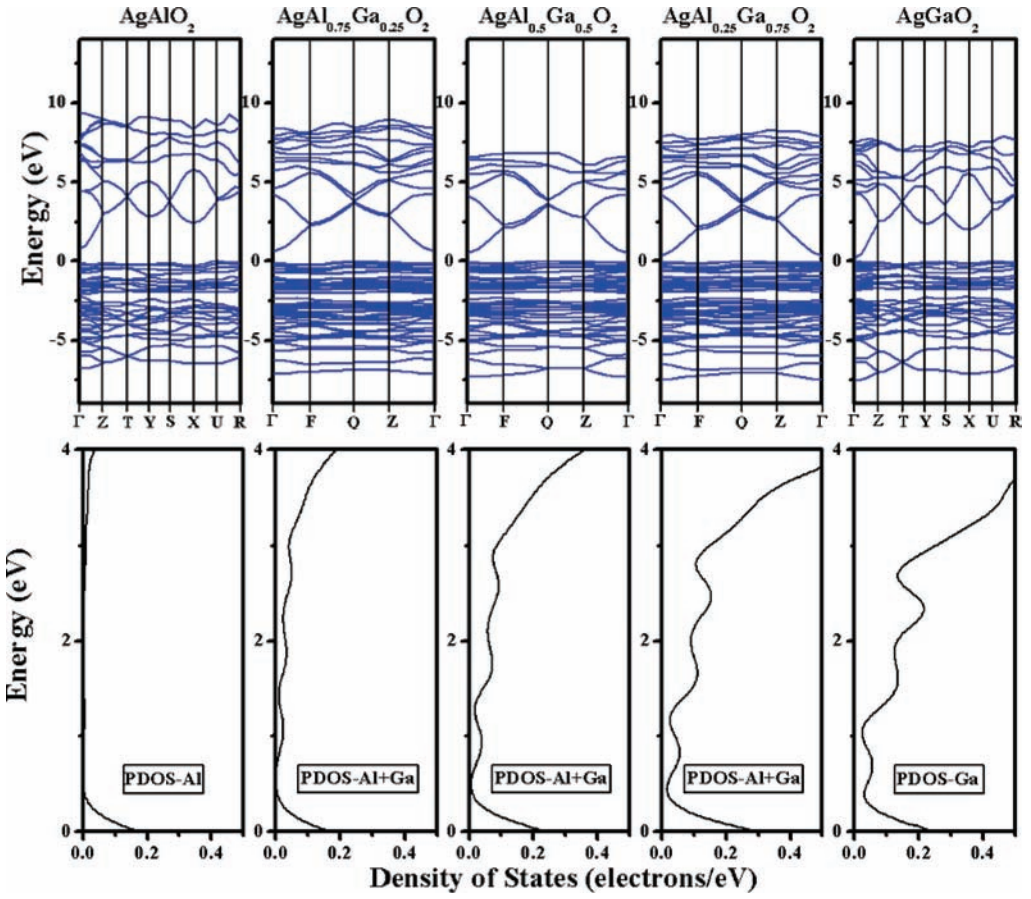

Figure 8. Electronic structures of β-$AgAl_{1-x}Ga_xO_2$ (x = 0, 0.25, 0.5, 0.75, and 1).

CBMs of $AgAlO_2$ and $AgGaO_2$ are calculated via Mulliken electronegativity[45,46] to be −0.638 and −0.253 eV (vs SHE), respectively, indicating that the CBMs of β-$AgAl_{1-x}Ga_xO_2$ solid solutions are more negative than the reduction potential of O_2 ($e^- + O_2 + H^+ \rightarrow HO_2$, −0.046 vs SHE).[47] Therefore, for IPA photodegradation over the present catalysts, the IPA is first oxidized by $\bullet O_2^-$ to generate acetone, thus the potential of CBM significantly affects the photocatalytic activity. The efficiency of β-$AgAl_{1-x}Ga_xO_2$ photocatalysts presents a maximum at x = 0.4, which can be reasonably attributed to the different construction in CB. On the basis of the band-structure characteristics of the present solid solutions, the lower level of CBM extends light absorption range in the visible region, but it generally suppresses the reduction potential. As an overall effect of the light absorption and the appropriate reduction potential, the β-$AgAl_{0.6}Ga_{0.4}O_2$ sample exhibits the highest activity for IPA photodegradation among these solid solutions. However, the absorption edge of this sample reaches only about 460 nm, which means that the material can harvest very limited visible light. Considering practical applications, further electronic-structure improvement should extend the light absorption of photocatalyst into a wider visible range to well match the solar spectrum and indoor-illumination spectrum and simultaneously achieve high apparent quantum efficiency in the wide visible region.

CONCLUSIONS

A new series of solid-solution photocatalysts, β-$AgAl_{1-x}Ga_xO_2$, was prepared by the cation-exchange reaction assisted by a sol−gel approach for generating Na-based solid-solution precursors. These solid solutions grow in a homogeneous crystal structure with orthorhombic symmetry but possess continuously modulated band gaps from 2.19 to 2.83 eV. The theoretical study demonstrates that the ratio of Ga/Al in the Ag-based solid solutions dominates the levels of conduction bands and, subsequently, the widths of the band gaps. All of these β-$AgAl_{1-x}Ga_xO_2$ solid-solution photocatalysts can degrade IPA under visible-light irradiation; in particular, the β-$AgAl_{0.6}Ga_{0.4}O_2$ sample shows the highest catalytic performance and achieves 37.3% of apparent quantum efficiency at the wavelength of 425 ± 12 nm, since its band structure adapts the balance of effective visible-light absorption and adequate redox potentials. The present work is evidence that fabricating solid-solution semiconductors with continuously tunable electronic structures is one of the most effective strategies to develop visible-light-sensitive photocatalysts with high performance.

ASSOCIATED CONTENT

Supporting Information. Flowchart of β-$AgAl_{1-x}Ga_xO_2$ synthesis; spectral profiles of Xe arc lamp with and without filters; geometry optimization to determine the most stable models for β-$AgAl_{0.75}Ga_{0.25}O_2$, β-$AgAl_{0.5}Ga_{0.5}O_2$, and β-$AgAl_{0.25}Ga_{0.75}O_2$; lattice parameters as a function of x in β-$AgAl_{1-x}Ga_xO_2$; SEM images of β-$AgAl_{1-x}Ga_xO_2$ samples; details of the conduction band bottom and the valence band top of β-$AgAlO_2$, β-$AgAl_{0.75}Ga_{0.25}O_2$, β-$AgAl_{0.5}Ga_{0.5}O_2$, β-$AgAl_{0.25}Ga_{0.75}O_2$, and β-$AgGaO_2$; photoactivities of β-$AgAl_{1-x}Ga_xO_2$ normalized by absorbed

photons; contrast optical properties between β-$AgAl_{0.6}Ga_{0.4}O_2$ and commercial $TiO_{2-x}N_x$; long-term experiment of IPA photooxidization over β-$AgAl_{0.6}Ga_{0.4}O_2$ under irradiation of blue-LED lamps; XRD patterns and UV−visible absorption spectra of as-prepared and postreaction samples; and calculation details of turnover number. This material is available free of charge via the Internet at http://pubs.acs.org.

AUTHOR INFORMATION

Corresponding Author
Jinhua.Ye@nims.go.jp

ACKNOWLEDGMENT

This work was partially supported by the World Premier International Research Center Initiative on Materials Nanoarchitectonics, MEXT, JST-MOST Strategic Japanese-Chinese Cooperative Programme and the MEXT Program for Development of Environmental Technology using Nanotechnology, Japan. S. Ouyang is grateful to Yingpu bi and Yuanjian Zhang for their assistance in the writing of this manuscript.

REFERENCES

(1) Hoffmann, M. R.; Martin, S. T.; Choi, W.; Bahnemann, D. W. *Chem. Rev.* **1995**, *95*, 69–96.
(2) Herrmann, J. M. *Catal. Today* **2005**, *34*, 49–65.
(3) Agrios, A. G.; Pichat, P. *J. Appl. Electrochem.* **2005**, *35*, 655–663.
(4) Robertson, P. K. J.; Bahnemann, D. W.; Robertson, J. M. C.; Wood, F. *The Handbook of Environmental Chemistry*; Springer: Berlin, Heidelberg, 2005; Vol. 2M: Environmental Photochemistry Part II, pp 367−423.
(5) Kudo, A.; Miseki, Y. *Chem. Soc. Rev.* **2009**, *38*, 253–278.
(6) Roy, S. C.; Verghese, O. K.; Paulose, M.; Grimes, C. A. *ACS Nano* **2010**, *4*, 1259–1278.
(7) Anpo, M.; Aikawa, N.; Kubokawa, Y.; Che, M.; Louis, C.; Giamello, E. *J. Phys. Chem.* **1985**, *89*, 5017–5022.
(8) Asahi, R.; Morikawa, T.; Ohwaki, T.; Aoki, K.; Taga, T. *Science* **2001**, *293*, 269–271.
(9) Sakthivel, S.; Kisch, H. *Angew. Chem., Int. Ed.* **2003**, *42*, 4908–4911.
(10) Zhao, W.; Ma, W.; Chen, C.; Zhao, J.; Shuai, Z. *J. Am. Chem. Soc.* **2004**, *126*, 4782–4783.
(11) Yu, H.; Irie, H.; Hashimoto, K. *J. Am. Chem. Soc.* **2010**, *132*, 6898–6899.
(12) Zou, Z.; Ye, J.; Sayama, K.; Arakawa, H. *Nature* **2001**, *414*, 625–627.
(13) Tang, J.; Zou, Z.; Ye, J. *Angew. Chem., Int. Ed.* **2004**, *43*, 4463–4466.
(14) Wang, D.; Kako, T.; Ye, J. *J. Am. Chem. Soc.* **2008**, *130*, 2724–2725.
(15) Tsuji, I.; Kato, H.; Kobayashi, H.; Kudo, A. *J. Am. Chem. Soc.* **2004**, *126*, 13406–13413.
(16) Yan, H.; Yang, J.; Ma, G.; Wu, G.; Zong, X.; Lei, Z.; Shi, J.; Li, C. *J. Catal.* **2009**, *266*, 165–168.
(17) Hitoki, G.; Takata, T.; Kondo, J. N.; Hara, M.; Kobayashi, H.; Domen, K. *Chem. Commun.* **2002**, *16*, 1698–1699.
(18) Maeda, K.; Takata, T.; Hara, M.; Saito, N.; Inoue, Y.; Kobayashi, H.; Domen, K. *J. Am. Chem. Soc.* **2005**, *127*, 8286–8287.
(19) Maeda, K.; Teramura, K.; Lu, D.; Takata, T.; Saito, N.; Inoue, Y.; Domen, K. *Nature* **2006**, *440*, 295.
(20) Zong, X.; Yan, H.; Wu, G.; Ma, G.; Wen, F.; Wang, L.; Li, C. *J. Am. Chem. Soc.* **2008**, *130*, 7176–7177.
(21) Wang, G.; Yang, X.; Qian, F.; Zhang, J.; Li, Y. *Nano Lett.* **2010**, *10*, 1088–1092.
(22) Hensel, J.; Wang, G.; Li, Y.; Zhang, J. *Nano Lett.* **2010**, *10*, 478–483.
(23) Ye, J.; Zou, Z.; Arakawa, H.; Oshikiri, M.; Shimoda, M.; Matsushita, A.; Shishido, T. *J. Photochem. Photobiol. A* **2002**, *148*, 79–83.
(24) Yin, J.; Zou, Z.; Ye, J. *J. Phys. Chem. B* **2003**, *107*, 4936–4941.
(25) Ye, J.; Zou, Z. *J. Phys. Chem. Solids* **2005**, *66*, 266–273.
(26) Yoshino, M.; Kakihana, M.; Cho, W.; Kato, H.; Kudo, A. *Chem. Mater.* **2002**, *14*, 3369–3376.
(27) Yao, W.; Ye, J. *J. Phys. Chem. B* **2006**, *110*, 11188–11195.
(28) Wang, D.; Kako, T.; Ye., J. *J. Phys. Chem. C* **2009**, *113*, 3785–3792.
(29) Li, G.; Kako, T.; Wang, D.; Zou, Z.; Ye, J. *J. Solid State Chem.* **2007**, *180*, 2845–2850.
(30) Ouyang, S.; Zhang, H.; Li, D.; Yu, T.; Ye, J.; Zou, Z. *J. Phys. Chem. B* **2006**, *110*, 1677–11682.
(31) Maruyama, Y.; Irie, H.; Hashimoto, K. *J. Phys. Chem. B* **2006**, *110*, 23274–23278.
(32) Irie, H.; Maruyama, Y; Hashimoto, K. *J. Phys. Chem. C* **2007**, *111*, 1847–1852.
(33) Ouyang, S.; Li, Z.; Ouyang, Z.; Yu, T.; Ye, J.; Zou, Z. *J. Phys. Chem. C* **2008**, *112*, 3134–3141.
(34) Ouyang., S.; Kikugawa, N.; Chen, D.; Zou, Z.; Ye, J. *J. Phys. Chem. C* **2009**, *113*, 1560–1566.
(35) Ouyang, S.; Kikugawa, N.; Zou, Z.; Ye, J. *Appl. Catal. A-Gen.* **2009**, *366*, 309–314.
(36) Yi, Z.; Ye, J.; Kikugawa, N.; Kako, T.; Ouyang, S.; Williams, H. S.; Yang, H.; Cao, J.; Luo, W.; Li, Z.; Liu, Y.; Withers, R. L. *Nat. Mater.* **2010**, *9*, 559–564.
(37) Kang, J. S.; Kwak, J. H.; Shin, Y. J.; Han, S. W.; Kim, K. H.; Min, B. I. *Phys. Rev. B* **2000**, *61*, 10682–10687.
(38) Ohko, Y.; Hashimoto, K.; Fujishima, A. *J. Phys. Chem. A* **1997**, *101*, 8057–8062.
(39) Arsac, F.; Bianchi, D.; Chovelon, J. M.; Ferronato, C.; Herrmann, J. M. *J. Phys. Chem. A* **2006**, *110*, 4202–4212.
(40) Segall, M. D.; Lindan, P. L. D.; Probert, M. J.; Pickard, C. J.; Hasnip, P. J.; Clark, S. J.; Payne, M. C. *J. Phys.: Cond. Matt.* **2002**, *14*, 2717–2743.
(41) Thompson, J. G.; Withers, R. L.; Palethorpe, S. R.; Melnitchenko, A. *J. Solid State Chem.* **1998**, *141*, 29–49.
(42) Butler, M. A. *J. Appl. Phys.* **1977**, *48*, 1914–1920.
(43) Abe, R.; Takami, H.; Murakami, N.; Ohtani, B. *J. Am. Chem. Soc.* **2008**, *130*, 7780–7781.
(44) Bell, A. T. *Science* **2003**, *299*, 1688–1691.
(45) Butler, M. A.; Ginley, D. S. *J. Electrochem. Soc.* **1978**, *125*, 228–232.
(46) Nethercot, A. H. *Phys. Rev. Lett.* **1974**, *33*, 1088–1091.
(47) Bard, A. J.; Parsons, R.; Jordan, J. *Standard Potentials in Aqueous Solution*; Marcel Dekker: New York, 1985; pp 49−66.